

Article

# Location- and Time-Specific Hydrological Simulations with Multi-Resolution Remote Sensing Data in Urban Areas

Charlotte Wirion <sup>\*,†</sup>, Willy Bauwens and Boud Verbeiren

Department of Hydrology and Hydraulic engineering, Vrije Universiteit Brussel (VUB), 1050 Ixelles, Belgium; wbauwens@vub.ac.be (W.B.); Boud.Verbeiren@vub.ac.be (B.V.)

\* Correspondence: Charlotte.Wirion@vub.ac.be; Tel.: +32-2629-3036

† Current address: Pleinlaan 2, 1050 Brussels, Belgium.

Academic Editors: Xin Li, Magaly Koch and Prasad S. Thenkabail

Received: 14 April 2017; Accepted: 16 June 2017; Published: 22 June 2017

**Abstract:** A major challenge in hydrologic modeling remains the mapping of vegetation dynamics in an urban landscape. The impact of vegetation on interception storage varies over time and needs to be quantified in order to enable proper management of water resources in urban areas. However, the heterogeneity and complexity of the urban landscape makes it challenging to monitor urban vegetation. A more detailed spatial and temporal scale is needed. To characterize surface cover at a high spatial resolution, a hyperspectral APEX image (2 m) is used, while a time series of Proba-V images (daily, 100 m) allows a detailed characterization of the seasonal variation of urban greenness. For this study, we use and validate the leaf area index (LAI) maps derived from APEX and Proba-V data for a selected pixel in the Watermaelbeek catchment in Brussels (Belgium). The ground-truthing of the Proba-V pixels includes a detailed mapping of land cover characteristics and more specifically vegetation cover throughout the seasons. LAI values calculated based on the APEX image agree with the LAI values measured from the ground ( $n = 106$ ,  $R^2 = 0.68$ ). Further, the aggregated APEX pixels correlate with the Proba-V pixels ( $R^2 = 0.79$ ), and the Proba-V data can be used to monitor vegetation dynamics. As the seasonal LAI measurements correspond with the Proba-V dynamics, we conclude that Proba-V images allow the characterization of vegetation dynamics at a high spatial resolution in heterogeneous areas. We create a time series of LAI maps at a high resolution (2 m), which allows a location- and time-specific simulation of interception storage and thus contributes to managing water resources in urban areas.

**Keywords:** Proba-V; APEX; NDVI; LAI; hydrological modeling

## 1. Introduction

The development of urban areas leads to a rapid transformation of land cover (e.g., vegetation, bare soil, water and man-made surfaces) and land surface properties (e.g., heat capacity, soil moisture, vegetation density and diversity, surface roughness) and therefore highly affects the energy and water cycles of these areas [1,2]. The reduction of vegetation cover, the sealing of surfaces and the construction of buildings and roads reduce the rainfall losses by interception, infiltration and evapotranspiration and thus increase the net rainfall amount available for storm runoff in urban catchments. Urbanized catchments are also a main cause for the pollution of water resources due to storm water runoff, combined sewer overflows and wastewater treatment plants [3]. As hydrologists start to consider not only the major rainfall events, but raise their interest for more common events, interception becomes important. It is crucial to determine new management strategies for urban vegetation in order to mitigate urbanization effects [3]. Thus, there is an increased need to simulate

the water fluxes in urban areas and quantify the impact of vegetation on the water fluxes [4]. As a consequence, monitoring the seasonal variations of urban vegetation and its impact on interception storage to quantify the influence on the urban water balance are crucial for sustainable city planning. The heterogeneous distribution of vegetation in urban catchments makes the characterization of vegetation and its potential benefits challenging. Therefore, we need hydrological models with a high spatial and temporal resolution to account for the high heterogeneity and fast dynamics of hydrological processes in urban areas [5]. This paper sets up such a model to simulate the impacts of vegetation on the interception storage of the Watermaelbeek catchment in Brussels, Belgium.

Urban hydrological models usually use land cover information based on GIS technologies, and only a few modelers take advantage of the spatial and temporal coverage of remote sensing (RS) techniques [6–8]. Remote sensing provides the possibility to classify surfaces objectively into land cover classes and to monitor seasonal dynamics, as well as the land use changes over a period of years. The potential of satellite data for field and regional planning is however limited by the challenge of translating its images into usable parameters [9]. The normalized difference vegetation index (NDVI) of multispectral imagery can be used to characterize vegetation in urban areas. As a physically meaningful parameter for hydrological modeling, the remotely-sensed leaf area index (LAI) improves simulation results [10,11]. The NDVI and LAI deduced from frequent satellite imagery are valuable as the seasonal variation of vegetation can be considered. However, the heterogeneous character of urban areas makes the use of satellite data challenging.

The potential of satellite imagery to describe the heterogeneity of urban catchments is limited due to its relatively coarse resolution [9,12,13]. Moreover, the derivation of the structural characteristics of the tree canopy remains difficult as optical imagery is limited to two dimensions. Finally, shadowing effects may increase the complexity of the classification [14]. The potential of light detection and ranging (LiDAR) methods in combination with multi-spectral remote sensing has been explored to improve classification results [14,15]. However, an accurate estimation of urban tree cover remains complex with LiDAR data [15]. Therefore, Launeau et al. [16] suggest using airborne hyperspectral and high resolution imagery to characterize trees in an urban environment. Several studies indicate improvements in describing functional vegetation properties [16–19]. In this study, we try to combine the high spatial resolution of the hyperspectral APEX (Airborne Prism EXperiment) image (2 m) with the high temporal resolution of the multispectral Proba-V (Project for OnBoard Autonomy-Vegetation) images (daily) to improve the parameterization of urban hydrological models.

The main objective is to create an LAI map time series at a high resolution, based on the combined RS data, for location- and time-specific estimation of interception storage. We compare hydrological simulations including the LAI map time series with simulations not using the LAI map time series to model interception storage.

## 2. Materials and Methods

### 2.1. Study Site

The study site is the Watermaelbeek (WMB) catchment, which represents the most urbanized part of the upper Woluwe catchment (see Figure 1), a tributary of the Senne River in Brussels, Belgium. The WMB catchment has an area of 7.2 km<sup>2</sup>. The elevation gradually decreases from the southwest to the northeast and ranges from 121 m to 54 m a.s.l. For the Watermaelbeek, the predominant soil type is well-drained loamy soil. The APEX coverage is illustrated in Figure 1 (left). Brussels has a temperate climate with moderate temperatures and an average rainfall of 853 mm/year [20]. Thus, cloud cover is an issue in this study area. The land cover is predominantly urban (residential), but the southeast of Brussels, where the upper Woluwe catchment is situated, still has a dense vegetation cover.

The meteorological inputs are based on hourly data for 2015 from the Royal Meteorological Institute of Belgium (RMI) for the Uccle station in the Brussels region. The RMI measures temperature, relative humidity, precipitation, wind direction and speed, as well as global and infrared radiation data.

The precipitation data are compared to pluviometer measurements at the *depot communal* under the supervision of Flowbru, a water monitoring network for the Brussels Capital Region [21], to investigate for outliers. The potential evapotranspiration is calculated using the Penman–Monteith equation [22].

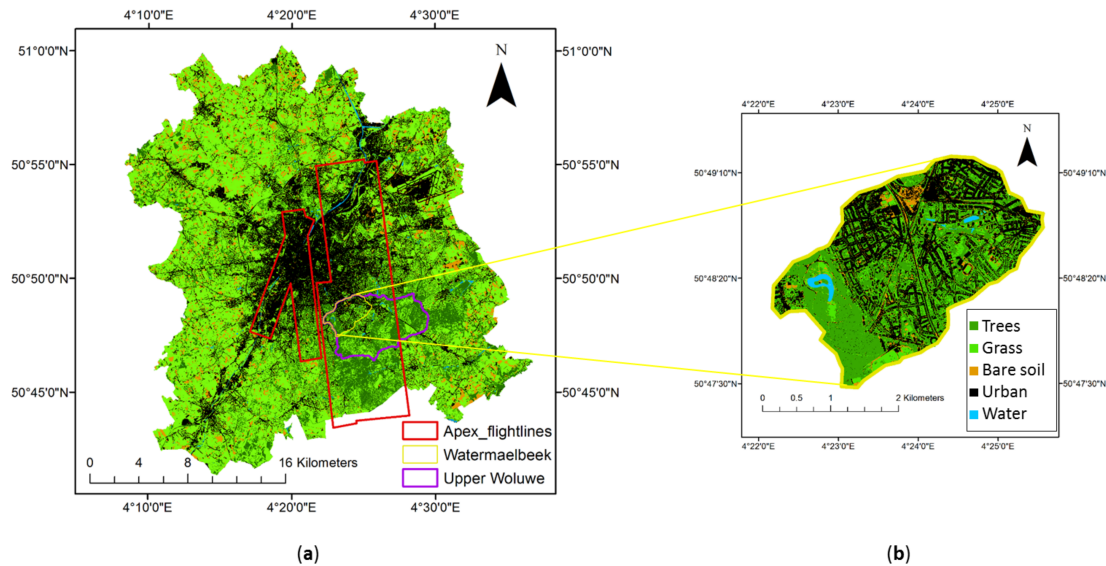


**Figure 1.** The Brussels region (a) with the study site (yellow), the APEX flight lines (red) and the upper Woluwe catchment (purple). The land cover of the WMB catchment is illustrated in the right panel (b). The urban fraction covers 39%, trees cover 36%, grass 17.3%, bare soil 6.5% and water 1.2% of the WMB catchment.

## 2.2. Field Data

For assessing the LAI from 106 individual trees in the urban catchment (see Section 2.1), the SunScan system (Type SS1-COM-R4) was used. The SunScan measures incident and transmitted photo-synthetically-active radiation (PAR). The trees were selected according to the position (isolated and within the APEX flight lines) and the species. The focus was on the 4 most common urban tree types in Brussels: maple (*Acer platanoides* and *pseudoplatanus*), birch (*Betula pendula*), chestnut (*Aesculus hippocastanum*) and linden (*Tilia*). As the height and structure of the trees are variable (see Table 1), the measurements were taken 1 m below the canopy in 8 compass directions of each studied tree. For each compass direction, the SunScan was positioned at a 1-m distance from the stem.

**Table 1.** Trees inventory ( $n = 106$ ).

Statistics	Maple	Birch	Chestnut	Linden
sample number	36	9	28	33
mean height (standard deviation)	15 m (5 m)	16 m (1 m)	16 m (6 m)	14 m (5 m)
mean DBH (standard deviation)	0.45 m (0.35 m)	0.40 m (0.05 m)	0.59 m (0.33 m)	0.38 m (0.21 m)
mean crown diameter (standard deviation)	10 m (6 m)	11 m (5 m)	10 m (4 m)	10 m (4 m)

Based on the Beer–Lambert Law and Norman and Jarvis [23] and Goudrian [24], we calculated LAI according to the following equation:

$$LAI = \frac{\left(1 - \frac{1}{2k}\right)f_b - 1}{A} \times \ln T \quad (1)$$

where  $T$  is the fraction of transmitted photo-synthetically-active radiation (PAR) defined by  $PAR_{belowcanopy}/PAR_{abovecanopy}$ , and  $fb$  is the beam fraction defined by  $PAR_{diffuse}/PAR_{direct}$ . The extinction coefficient  $k$  is modeled as:

$$k = \frac{\sqrt{x^2 + \tan^2 \theta}}{x + 1.744 \times (x + 1.182)^{-0.733}} \quad (2)$$

and  $\theta$  is the solar zenith angle in degrees. The leaf angle distribution is assumed to be spherical ( $x = 1$ ). John Norman [25] set up the equation  $A = 0.283 + 0.785a - 0.159a^2$  where  $a = 0.85$  is the SunScan leaf absorptivity.

The ground-truthing of RS data included a detailed mapping of land cover characteristics and more specifically vegetation cover throughout the seasons. To measure the  $PAR_{abovecanopy}$ , a sunshine sensor (Type BF5) was used, and the total and diffuse incoming radiation were measured simultaneously outside and below the canopy. The LAI of 106 trees throughout the APEX flight lines was measured within 1 month of the flight, and the seasonal dynamics of 18 trees within one Proba-V pixel were monitored on the Vrije Universiteit Brussel (VUB) campus in Brussels, Belgium, from April to October 2015 (Figure 2). The VUB campus is situated adjacent to the northern part of the WMB catchment. The trees represent 28% of the pixel, whereas grass covers 39%, bare soil 3%, and another 30% of the pixels is impervious.

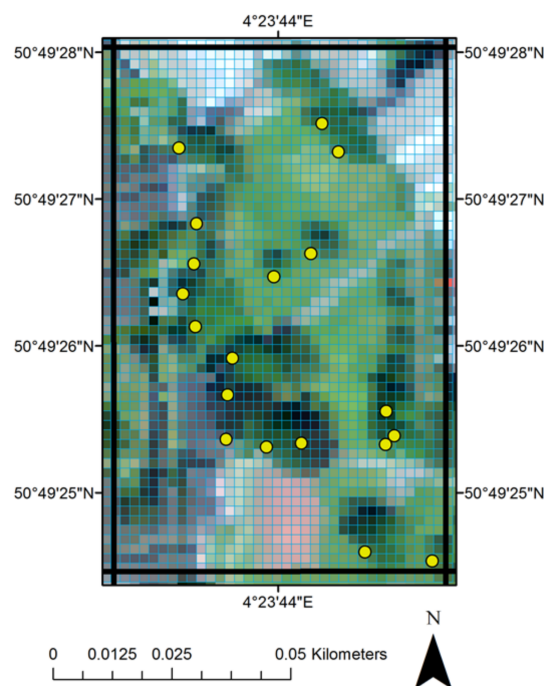


**Figure 2.** Selected Proba-V pixel with 18 monitored trees (yellow dots). The Proba-V pixel is delineated by the black lines (110 × 70 m), whereas the APEX pixels are delineated with blue lines (2 × 2 m).

### 2.3. Remote Sensing Data

The airborne hyperspectral APEX image (Airborne Prism Experiment) with a 2 m resolution was taken on 30 June 2015 within the framework of the Belair 2015 campaign (<http://belair.vgt.vito.be/content/belair-2015>). The 5-day Proba-V products for Belgium (PV\_S5\_TOC\_100M) were downloaded for April to October 2015. Proba-V provides 5-day products, summarized from daily products, to provide more cloud-free images at the 100m spatial resolution. For that period only 10 cloud-free images are covering the study area (11 April 2015, 16 April 2015, 21 April 2015, 26 April 2015, 1 June 2015, 11 June 2015, 11 July 2015, 1 August 2015, 26 August 2015, 1 October 2015). To compare

the Proba-V with aggregated APEX pixels, the image from 1 July 2015 was selected. The image of 1 July was selected as it is closest to the APEX flight-time and the clouds on the image do not directly overlap the flight-lines. However, as we can not exclude all cloud effects, the image was not used for creating an LAI timeseries. The Proba-V images were reprojected from GCS-WGS-84 to Belgian Lambert 72 coordinates, which implied a transformation of the originally squared pixels to rectangular pixels (from  $100 \times 100$  m to  $70 \times 110$  m).

The generation of the urban land cover map was based on an airborne hyperspectral APEX image with a 2-m resolution. Based on 200 known pixels per class, so-called training pixels, a supervised classifier, the support vector machine (SVM) classifier, was applied to the APEX image. Thirty one subclasses such as impervious roofing and pavements (tiles, asphalt, concrete) or pervious vegetated (trees, shrubs, grasses) and non-vegetated surfaces (water, bare soil) were used to generate the high-resolution land cover map of the Watermaelbeek catchment. The classification results are further elaborated in [14] presenting an overall kappa value of 0.87 in sunlit and 0.69 in shaded areas. The kappa coefficient was used as a measure of agreement between the classification results and a set of shaded and sunlit validation polygons. Figure 1 (right) illustrates a simplified land cover map of the Watermaelbeek catchment. The impervious fraction covers 39% (roofing materials 22% and pavements 17%) of the WMB catchment, whereas trees cover 36%, grass 17.3%, bare soil 6.5% and water 1.2%.

To monitor the seasonal variation of the vegetation within the WMB, the 5-day Proba-V products were taken and disaggregated from the seasonal LAI to the spatial resolution of the APEX image (Figure 3). To create LAI maps based on APEX and Proba-V data, the normalized difference vegetation index (NDVI) (Equation (3)) is calculated according to Tucker [26].

$$NDVI = \frac{NIR - RED}{NIR + RED}. \quad (3)$$

Proba-V defines for the red (*RED*) and near-infrared (*NIR*) bands the following wavelength: *RED* = 655 nm and 79 nm width and *NIR* = 845 nm and 144 nm width. Therefore, the following APEX bands for the calculation of NDVI: Bands 30 to 56 (656.5 nm and 81 nm width) for *RED* and Bands 76 to 100 (847.5 nm and 145 nm width) for *NIR*. Based on the findings of [27], the LAI (Equation (4)) is calculated based on the NDVI maps and using the method of Su [28].

$$LAI = \sqrt{NDVI \times \frac{1 + NDVI}{1 - NDVI}} \quad (4)$$

Bindhu and Narasimhan [29] developed a disaggregation method (DisNDVI) for generating a time series of NDVI images aiming at a spatial resolution of 60 m. For this study, we created LAI maps with a spatial resolution of 2 m (Figure 3). At this resolution, we have 1 APEX image available for the study area. We aggregated the APEX pixels to the Proba-V resolution and created land cover fractions within the 100-m resolution Proba-V pixels. Dynamic land cover types were identified by generating seasonal NDVI and LAI profiles of homogeneous Proba-V pixels. Homogeneous Proba-V pixels were defined for trees and impervious surfaces if >90% of the Proba-V pixel is covered by one of these land cover types. For grass, not enough pixels with >90% coverage are present in our study area. To obtain a similar number of homogeneous Proba-V pixels a threshold of >50% was selected. Stable versus dynamic land covers were defined by comparing the seasonal trend per land cover type. Land cover types without a clear seasonal trend were considered stable land cover types. To create LAI maps at 2-m resolution, the stable land cover fractions use the constant LAI values (averaged throughout the year based on homogeneous Proba-V pixels), whereas the dynamic land cover types use the LAI values of the Proba-V images throughout the season. To disaggregate the LAI values of the Proba-V image to the APEX resolution, the weighted LAI for the given Land Cover 1 (*LC1*) was derived as occupying the fraction ( $frac_{LC1}$ ) of the Proba-V pixel by subtracting the sum of the weighted LAI's from the other land cover types (e.g., *LC2*, *LC3*) from the LAI of the Proba-V pixel ( $LAI_{Proba-V}$ ), as shown in Equation (5).

$$LAI_{LC1} = LAI_{Proba-V} - (frac_{LC2} \times LAI_{LC2} - frac_{LC3} \times LAI_{LC3}) / frac_{LC1} \quad (5)$$

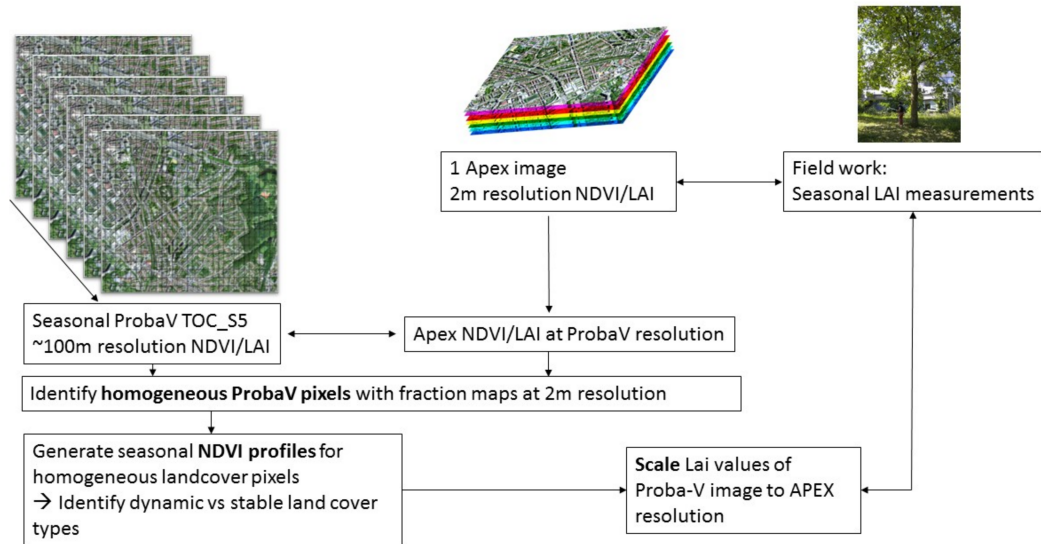


**Figure 3.** Monitoring urban vegetation dynamics based on RS products and ground-truth validation.

#### 2.4. The Water Balance Model: WetSpa

The Water and Energy Transfer between Soil Plants and Atmosphere simulator (WetSpa) [30,31] allows a detailed modeling of the land surface processes. For this study, the focus is on WetSpa's capacity for simulating the interception storage at the surface in a continuous and distributed manner. A more recent version of WetSpa was developed in view of the application in urban areas [32] (Table S1). This version increases the flexibility of the different model components in that every physically-based process is coded in a separate module, and every component can have a different spatial and temporal resolution. This allows one to account for the heterogeneous distribution of urban greenness and the seasonal effects of the vegetation. The interception module is an important first step in the modeling process, as it determines the amount of net rainfall that is actually available for the calculation of the remaining components of the water balance. It calculates net rainfall by reducing the rainfall amount until the interception storage capacity is filled. The classical approach to simulate the interception storage with WetSpa uses a sine curve to interpolate between minimum and maximum interception storage capacity values retrieved from the literature. With the approach used here, LAI maps were integrated into the WetSpa model for the estimation of interception storage capacity. A 2-m resolution and hourly time step were selected for one growing season (April to October 2015) and for the Watermaelbeek catchment. The spatially-distributed and seasonal LAI maps were created for each simulation time step within the WetSpa model using linear interpolation between the selected Proba-V images. To create a yearly water balance, 2 additional Proba-V images were selected: one to define minimum conditions before the growing season starts (6 March 2015) and the other to define minimum conditions after the growing season ends (21 November 2015). The interception storage capacity for trees is calculated using the formula for broad leaf forest trees (Equation (6)), whereas a specific formula is used for the interception of grass and shrubs (Equation (7)) [33]. It is known that those equations are empirical and might not be fully applicable to our case. There is a lack of validated equations for our study area, and research is ongoing to fill this gap.

$$I_{max} = 1.184 + 0.490 \times LAI \quad (n = 5, R^2 = 0.76) \quad (6)$$

$$I_{max} = 0.3063 \times LAI + 0.5753 \quad (n = 6, R^2 = 0.82) \quad (7)$$

where  $I_{max}$  is the interception storage capacity, and  $n$  represents the sample number to set up the equation. WetSpaClassic refers to the classical approach of the WetSpa model, whereas WetSpaLAI refers to the new approach including dynamic LAI maps.

### 3. Results

#### 3.1. The Ground-Truthing of the High Resolution LAI Map Based on the APEX Image

Figure 4 shows that the LAI calculated based on the APEX image corresponds to the LAI measured on the ground with a correlation of 0.68 and a root mean squared error of 0.2 ( $n = 106$ ). The mean of ground-truth and APEX LAI is 3.0. The median is 2.9 for the ground-truth and 3.0 for the APEX LAI. For the minimum LAI, the values from the APEX image are almost double the ground-truth LAI values (Figure 4). The differences between the two datasets are explained as follows: The APEX image taken from the sky includes the land cover below the trees and is incorporated into the LAI calculation. For trees with sparse canopies the position of the tree (on grass, asphalt, concrete) impacts the spectral reflectance, and thus, a tree with a similar canopy can have higher LAI values if situated on grass. Further considering the maximum, ground-truth LAI is higher than APEX LAI. The ground-truth measurements are influenced by shadow in the urban environment, the weather conditions of the day and a shift in time (time of flight  $\pm 1$  month). For the trees where the SunScan indicates an LAI that is almost double the APEX LAI, we observed flowering, pruning and rust on leaves during the ground-truth measurements.

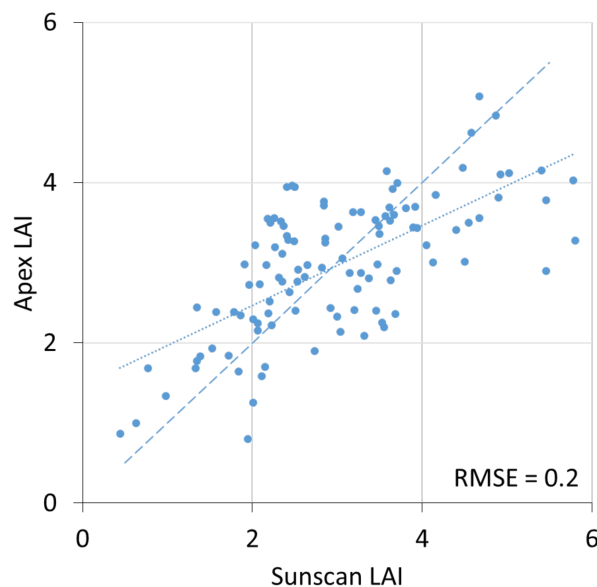


**Figure 4.** Scatter plot of measured LAI (x-axis) vs. APEX LAI (y-axis) for 106 trees. Linear regression as the dotted and 1:1 as the dashed line.

#### 3.2. The Aggregation of APEX NDVI/LAI to Proba-V Resolution and Ground-Truthing of Proba-V Products

In order to select homogeneous pixels within the seasonal Proba-V data, we aggregate the APEX image to the Proba-V resolution (100 m). We then define the fractions occupied by different land cover types within each Proba-V pixel. Homogeneous Proba-V pixels are selected to analyze the

seasonal dynamics of different land cover types. To validate the aggregation process, we compare the NDVI values of the Proba-V pixels with the aggregated APEX NDVI pixels. Figure 5a shows that we find a good correlation between the NDVI of Proba-V and the NDVI of the aggregated APEX map ( $R^2 = 0.79$ ). Data are attributed to the differences in the spectral band width and differences in image processing between Proba-V and APEX images. Further, more clear sky was present on the acquisition date of APEX (30 June 2015) than on the date of the chosen Proba-V image (1 July 2015). Figure 5b illustrates that the dominant land cover classes are grouped according to the expected NDVI values: low for the selected homogeneous Proba-V pixels with >90% impervious cover ( $n = 35$ ), moderate with >50% grass cover ( $n = 18$ ) and high with >90% tree cover ( $n = 24$ ). As the grass pixels are not as homogeneous as the impervious and tree pixels, we observe a bigger spread of the NDVI values. However, we obtain an average NDVI of 0.7 for grass, which corresponds to the NDVI values for urban grass found in the literature [34]. As within the impervious pixels, 10% are not covered by urban materials, the NDVI is not zero, but averages to 0.2.

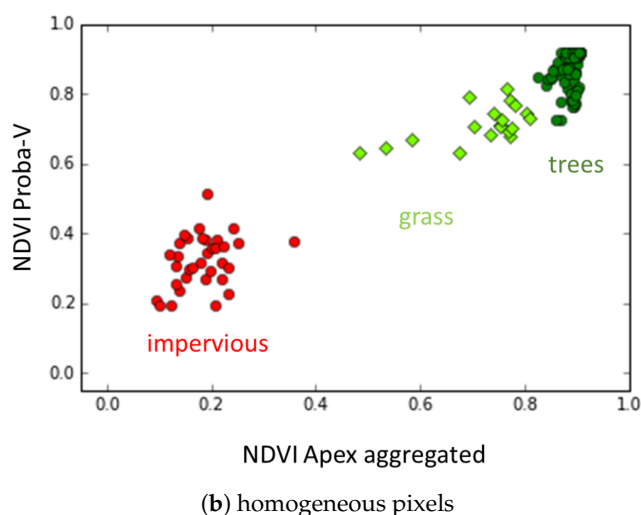
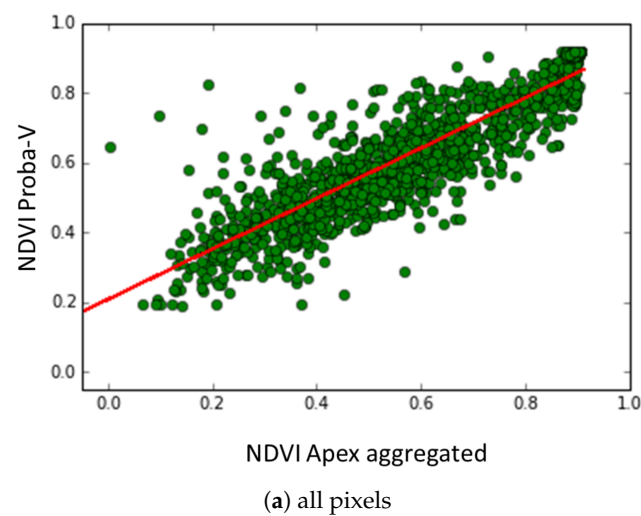


**Figure 5.** Proba-V vs. aggregated APEX NDVI values for the Watermaelbeek catchment for (a) all pixels and (b) homogeneous pixels.

In the next step, the seasonal dynamics of the selected homogeneous pixel classes were analyzed using one Proba-V image per month from April to October 2015. An average value over all

homogeneous pixels from a dominant land cover type was taken. Figure 6 illustrates that the Proba-V pixels with >90% of tree coverage show seasonal dynamics (polynomial fit,  $R^2 = 0.67$ ), whereas neither the impervious (polynomial fit,  $R^2 = 0.92$ ), nor the grass pixels (polynomial fit,  $R^2 = 0.35$ ) show this seasonality. The grass and impervious pixels show a trend similar to the trees pixels, but less pronounced, as a percentage within the homogeneous Proba-V pixels can be covered with trees (maximum 49% in grass pixels and 9% in impervious pixels). The grass pixels are deviating more from the curve than the impervious pixels because of management (growing/mowing). For the following steps, we assume all land cover fractions without trees to have a constant yearly mean (grass = 0.7,  $R^2 = 0.59$  and impervious = 0.2,  $R^2 = 0.86$ ). The LAI variation within the Proba-V pixel is only influenced by the dynamics of the tree canopies within that pixel.

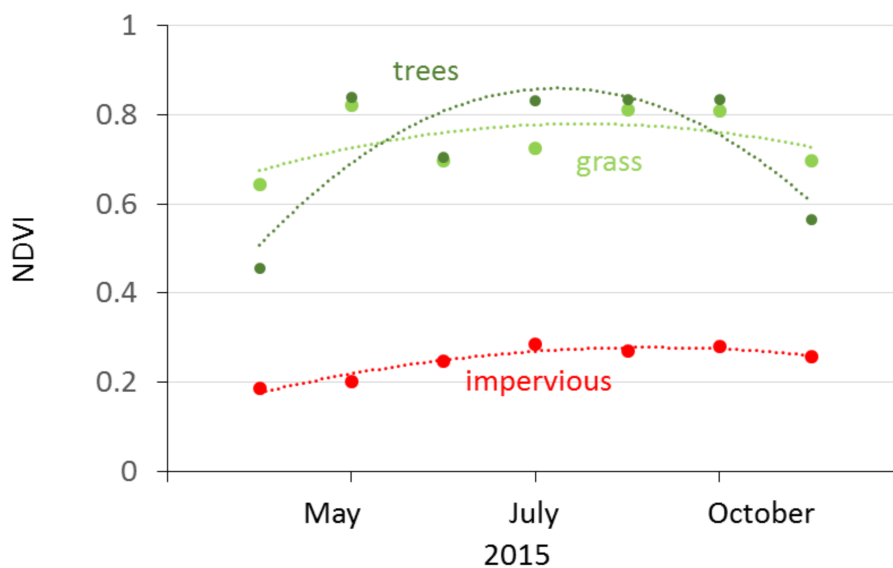


**Figure 6.** Seasonal dynamics of homogeneous Proba-V pixels from April to November 2015.

Finally, the seasonal dynamics of a Proba-V pixel are compared to the measured dynamics of 18 trees within that specific pixel (Figure 2). Figure 7a illustrates the LAI value for the given Proba-V pixel throughout the season as compared to the measured LAI values scaled to the Proba-V pixel resolution, including all land cover types within the pixel. As only 28% of the pixel is covered by trees, the LAI values are low, and the seasonal dynamics are unclear. Focusing only on the tree fraction within the pixel, the scaling approach described by Equation (5) is applied. Based on Proba-V, the LAI values vary from 2.5 to 4.5, whereas the field measurements result in LAI values from 0.6 to 4.2 from minimum (April and October) to maximum (May, June, July, August) conditions (Figure 7b). The difference of LAI for minimum conditions is due to the increasing influence of grass growing underneath on the LAI value of the Proba-V image as trees lose their leaves. The field measurements on the other hand are independent of undergrowth, but strongly influenced by the weather conditions during the day of measurements. The small drops in the curve (29 July 2015, 9 October 2015) are related to poorer weather conditions during measurements.

The agreement in the ground-truthing results of APEX and Proba-V LAI allows us to construct dynamic LAI maps based on the seasonal Proba-V data and with the spatial resolution of the APEX image (2 m). The scaling approach is used to attribute to each APEX pixel with a specific land cover the seasonal LAI value based on Proba-V. Based on the high resolution land cover map (Figure 1), urban materials, grass, bare soil and water pixels remain constant, whereas tree pixels vary throughout the season. Figure 8 illustrates an LAI map for minimum conditions (January 2015) (Figure 8a) and maximum conditions (July 2015) (Figure 8b). The maps illustrate that the LAI values change throughout the season not only in the forested park area (southwest), but also in the residential areas.

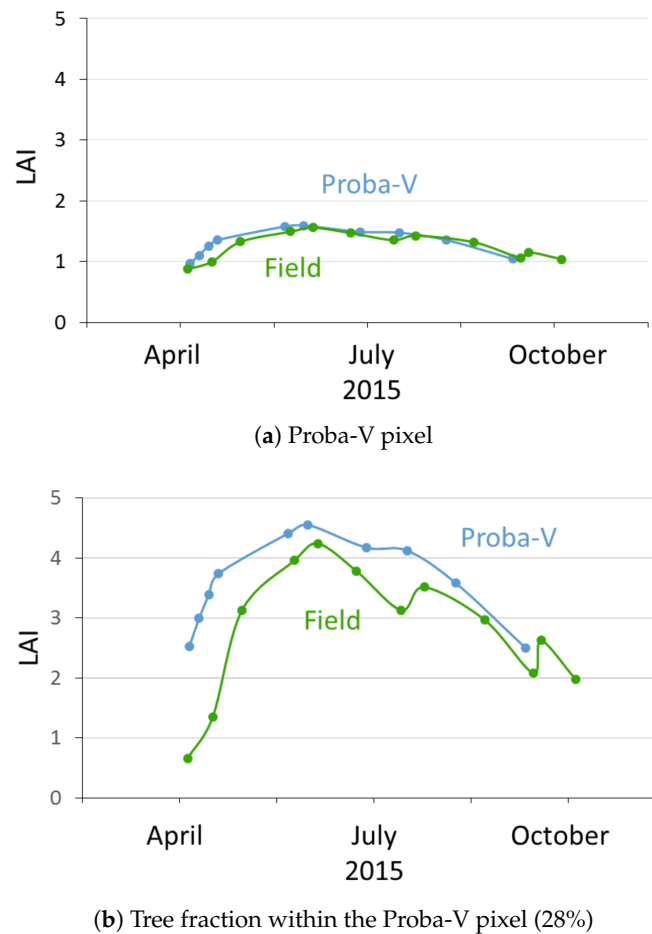


**Figure 7.** LAI dynamics of (a) the selected Proba-V pixel and (b) the tree fraction within the Proba-V pixel (28%) at the Vrije Universiteit Brussel (VUB) campus, Brussels, Belgium.

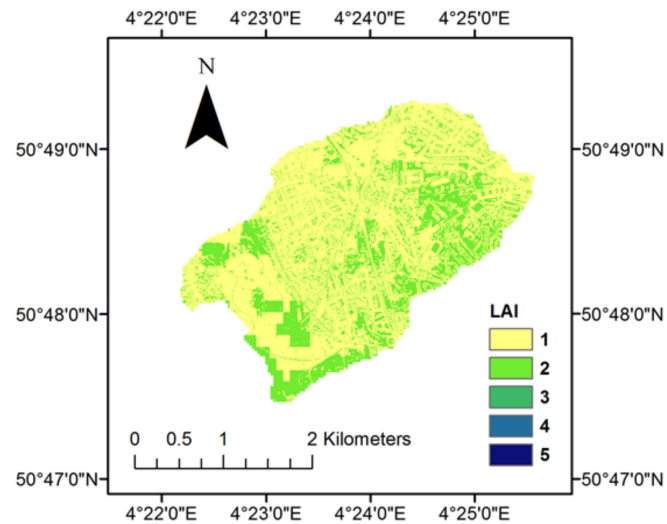
### 3.3. The Calibration and Validation of the WetSpa Model

The WetSpa model was calibrated for the Watermaelbeek catchment at a 2-m resolution for a six-month period (January, March, May, July, September, November 2015). The WetSpa simulations do not consider the influence of the sewer system, and thus, simulated low flows are not comparable to observed discharge data. Therefore, we use an adapted version of the Nash–Sutcliffe efficiency (NSE) to evaluate our model simulations (Equation (8)); with  $Q_s$  and  $Q_o$  being the simulated and observed runoff data per time step  $i$  [31].

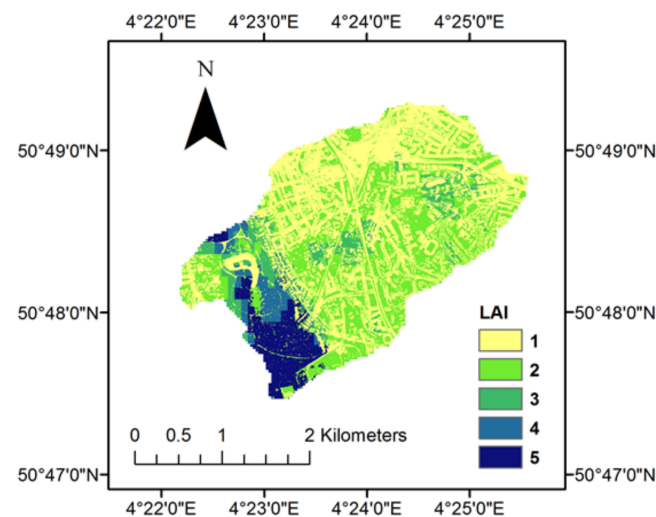
$$NSE = 1 - \frac{\sum_{i=1}^N (Q_{o_i} + \overline{Q_o})(Q_{s_i} - Q_{o_i})^2}{\sum_{i=1}^N (Q_{o_i} + \overline{Q_o})(Q_{o_i} - \overline{Q_o})^2} \quad (8)$$

The base flow is approximated by fitting a trend-line throughout the discharge data. In addition to the sewer infrastructure, the presence of a reservoir at the Watermaelbeek outlet affects the discharge time series at high intensity rainfall events. As rainfall flows into the reservoir, observed peak flows are lower than the simulations where the reservoir infrastructure is not accounted for. The behavior of the reservoir could not be simulated with WetSpa, and therefore, we remove 16 major events (event dates: 3 January, 8 January, 10 January, 15 January, 28 January, 29 March, 3 May, 4 May, 29 May, 5 June, 13 August, 15 August, 1 September, 13 September, 14 September, 19 November 2015). As the water

release from the reservoir is manually controlled, it is difficult to detect and account for the effect of water release on the observed discharge time series. This effect is not taken into account and will be reflected in the NSE values. We used an automated parameter estimation (PEST) [35], as well as a manual fine-tuning to calibrate the global parameters. The high spatial resolution (2 m) generates long computational times (two days/run), and therefore, we are satisfied with good NSE values for the calibration. The Nash–Sutcliffe efficiency (NSE) for the calibration is 68%. The validation period covered six months (February, April, June, August, October, December 2015), where we get an NSE value of 71% for both WetSpaClassic and WetSpaLAI. Regarding the water balance simulation, the model performs with a volumetric efficiency of 99.9%.



(a) LAI at minimum conditions (November 2015)



(b) LAI at maximum conditions (July 2015)

**Figure 8.** Seasonal LAI maps at (a) minimum conditions (November 2015) and (b) maximum conditions (July 2015) for the WMB catchment, Brussels, Belgium.

### 3.4. Introducing LAI Maps into the WetSpa Model

The interception capacity and actual interception storage are simulated with WetSpaClassic and WetSpaLAI for the WMB catchment. Figure 9 illustrates the interception storage capacity values averaged over all of the pixels within the WMB catchment for each time step. An increase of interception storage capacity to the peak capacity on 15 June followed by a decrease until the minimum conditions is the consequence of using a sine function (Figure 9, green curve). By introducing the LAI maps into the model, the peak interception storage capacity is reached in the beginning of June and then stays relatively constant until the end of the season where the capacity quickly drops to its minimum conditions (Figure 9, orange curve). WetSpaLAI allows linking interception storage capacity to a specific period (season, year) and location (WMB, Brussels), whereas WetSpaClassic only links the interception storage capacity to standard literature-based land cover conditions. Figure 9 clearly shows that the start of the vegetation season occurred later and was prolonged later. This is due to moderate temperatures in autumn and winter (the average temperature in November was 10 °C in 2015 vs. 6 °C for the long-term average [20]). Further, the maximum and minimum interception storage capacity threshold values used within the WetSpaClassic simulator are respectively higher and lower than the values we calculate based on LAI data. The main differences are that within the LAI approach, low vegetation (grass and shrubs) are considered having a constant interception storage capacity throughout the season ( $LAI = 0.7, I_{capacity} = 0.79 \text{ mm}$ ), whereas the classical WetSpa simulator varies the interception capacity of low vegetation from 0.5 to 2 mm. This lowers the interception storage capacity in winter months and increases the capacity in summer months. Further, the classical approach assumes a minimum value of 0.5 mm in minimum conditions for high vegetation (trees), whereas the LAI approach accounts for the different possible undergrowth (grass vs. impervious) and different types of trees (coniferous vs deciduous). This explains why the interception storage capacity is higher in minimum conditions using the new WetSpaLAI simulator.

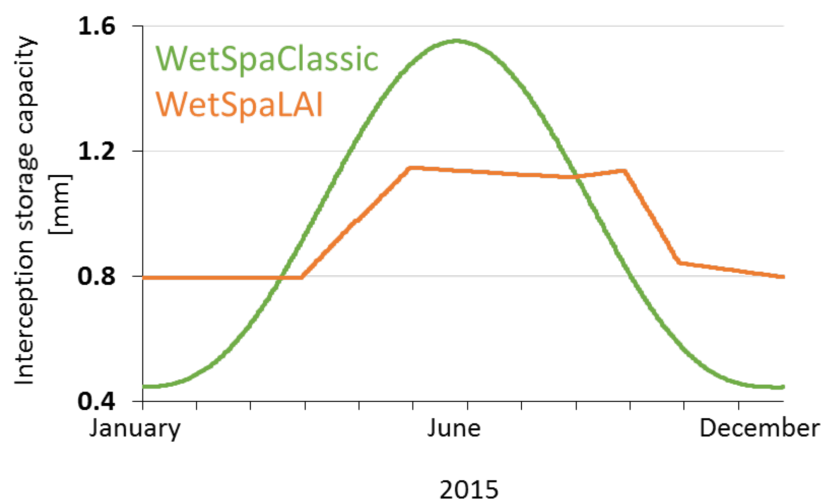


**Figure 9.** Comparison between WetSpaClassic and WetSpaLAI for the seasonal dynamics of the interception storage capacity for the Watermaelbeek in 2015.

In 2015, 709 mm of rainfall were recorded within the WMB catchment, 421 mm in winter (January to March and October to December) and 288 mm in summer (April to September) (Figure 10). For the WMB catchment, WetSpaClassic and WetSpaLAI simulate an annual interception storage of around 10% of the rainfall volume. This is comparable to the interception storage estimated for the Upper Woluwe catchment in 2010 to 2011 [27]. In winter, WetSpaLAI simulates an interception storage of 6% and WetSpaClassic of 5% of the rainfall water. In summer, the interception storage represents 16% with WetSpaLAI and 18% of the rainfall with WetSpaClassic. Further, WetSpaLAI indicates fewer net

rainfall events than WetSpaClassic for the WMB catchment in 2015. WetSpaLAI suggests that 80% of all rainfall events contribute to the 10% of the intercepted rainfall water. WetSpaClassic suggests that only 74% of the rainfall events contribute to the same amount of intercepted water. The needs and magnitude of rainfall removal by interception are thus different depending on the method applied and the seasons considered.

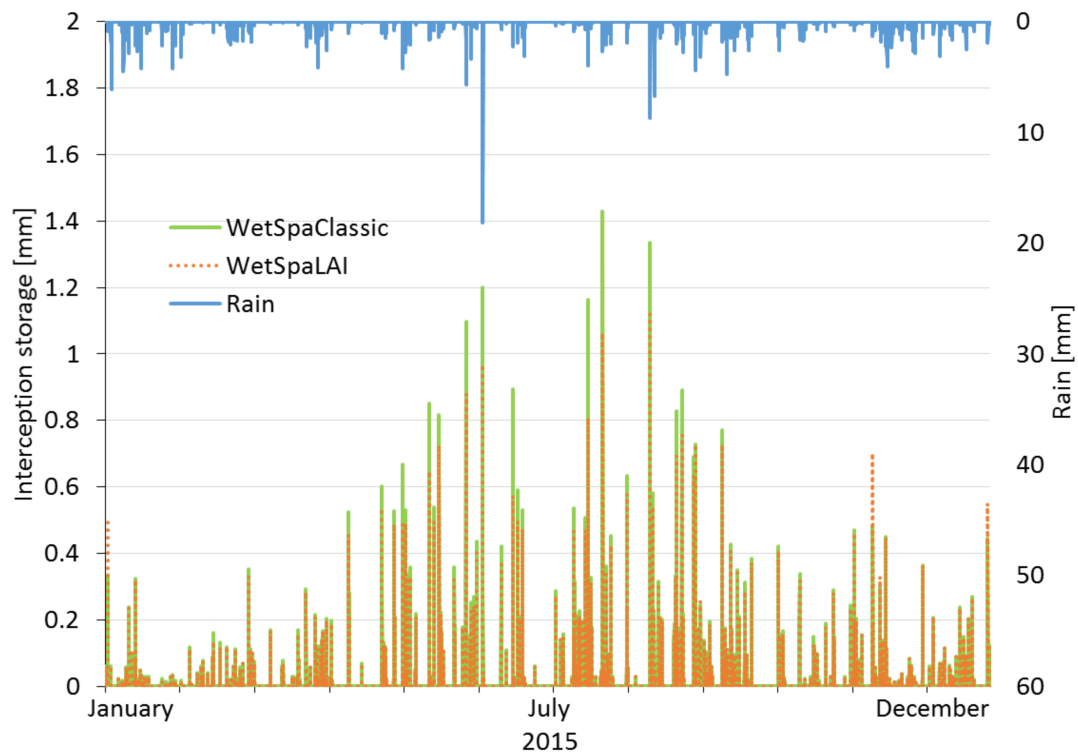
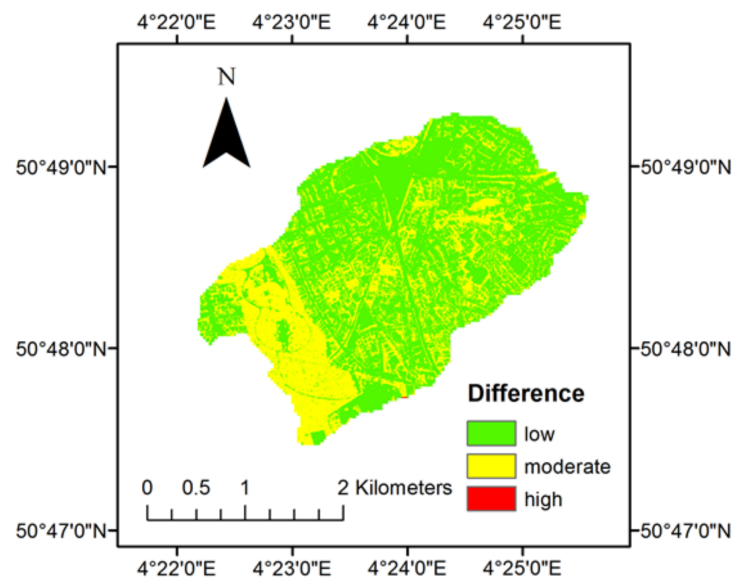
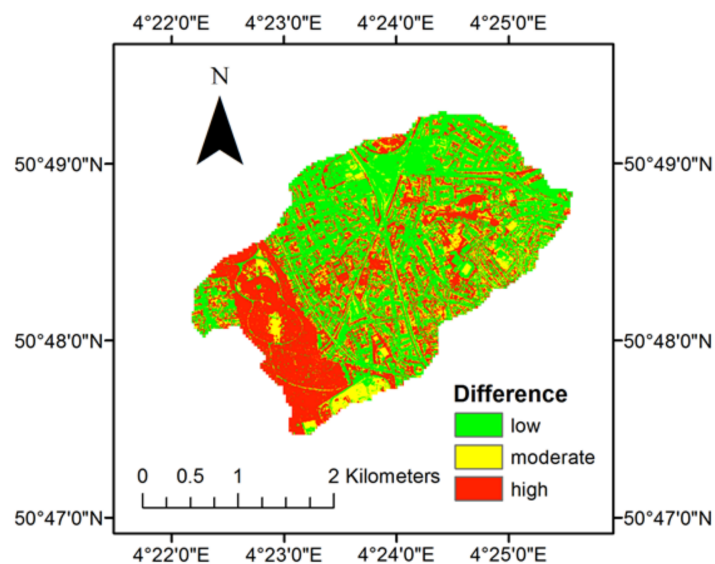


**Figure 10.** Comparison between WetSpaClassic and WetSpaLAI for the interception storage for the Watermaelbeek in 2015. In winter, WetSpaLAI shows higher interception storage, and in summer, WetSpaLAI shows lower interception storage than WetSpaClassic.

In Figure 11, we consider the spatially-distributed differences between WetSpaClassic and WetSpaLAI. The differences in interception storage for the tree-covered areas are more important in summer (15 mm difference, lower for WetSpaLAI) than in winter (3 mm difference, higher for WetSpaLAI). In winter, frequent rainfall events occur over short time periods, and potential evapotranspiration is low. As a result, there is insufficient time to empty the storage water in the trees, and the interception storage for the following event is limited. Thus, for many events, the difference between WetSpaClassic and WetSpaLAI in actual interception storage is minimal. In summer, as evapotranspiration is more important, the interception storage capacity is emptied more frequently, enabling multiple and consecutive interception to occur. Therefore, the differences between the two models become more explicit.



(a) Winter.



(b) Summer.

**Figure 11.** Spatially-distributed comparison between WetSpaClassic and WetSpaLAI for interception storage for the Watermaelbeek in 2015 (low <3 mm, moderate <5 mm, high <15 mm, absolute values). (a) January to March and October to December represent winter (WetSpaLAI higher). (b) April to September represent summer (WetSpaLAI lower).

#### 4. Discussion

##### 4.1. The Parameterization of Urban Trees with RS Data to Quantify the Impacts of Vegetation on Hydrological Processes

Temporally- and spatially-distributed LAI maps were created to obtain a location- and time-specific parameterization of urban trees. To obtain detailed and more accurate information, we combined a high spatial resolution land cover map based on an airborne RS image (APEX) with high temporal resolution satellite data (Proba-V). The drawback of disaggregating the Proba-V signal

to an APEX resolution is that the same NDVI is assigned to each urban tree fraction within the Proba-V pixel, and thus, an averaged signal is spread over all APEX pixels within one Proba-V pixel. Further, using the airborne APEX image is costly and limits the spatial and temporal coverage. Therefore, other, free alternatives should be considered for this type of analysis. The multispectral Sentinel 2 data could be an alternative as they have a spatial resolution of 20 m and a temporal resolution of 10 days. Further, it has been shown that hyperspectral data allow a higher accuracy for urban land cover mapping [36], and thus, EnMAP (Environmental Mapping and Analysis Programme) might be another solution to create very detailed and accurate land cover maps for urban areas. However, considering the temporal resolution, it is already a challenge to have enough cloud-free images to cover the growing season with the daily Proba-V images; thus, with Sentinel 2 (10 days coverage) and EnMAP (four days of coverage), it will remain an even greater challenge.

Within this paper, we characterized urban trees with their heterogeneous distribution throughout a city, as well as the seasonal changes. The difference in interception storage between the classical approach and the LAI module is not as important on an annual basis for the WMB catchment in 2015. However, if we look at specific events or seasonal trends, an important difference in interception storage is seen between the two simulations (Figure 10). Our study shows that the possibility to parameterize urban vegetation at a high spatial and temporal resolution can make the simulation of interception storage in urban areas location and period specific. For sustainable city planning, this method based on RS data can be of high value in order to monitor the impact of vegetation for reducing water quality and quantity issues, by reducing the net rainfall amount, as well as heat island effects by increasing local evapotranspiration. Different plant selection strategies can be developed to adapt the interception storage capacity to location-specific needs [37,38]. The new WetSpa simulator including LAI maps is location- and time-specific and thus accounts for different cases and scenarios.

#### *4.2. The Potential and Limits of RS Data for Hydrological Modeling in Urban Areas*

The WetSpa simulator calculates the water balance for each pixel and simulates hydrological processes using a cascade approach. The RS-driven approach allows for a spatial and temporal analysis of various water balance components. Our approach intends to characterize the urban land cover in great detail and get more physically-based estimates of the hydrological parameters to increase the credibility of the simulations. So far, we focus on the parameterization of urban vegetation and interception storage. Further steps within this research are to characterize hydrological parameters related to urban built-up land cover and to evaluate the effect on all water balance fluxes. Similarly, Sutanto et al. [39] focused on the water fluxes in the vadose zone to improve ET estimation, and Tang et al. [40] evaluate the retention capacity of infiltration rain gardens. Further, Liu et al. [41] assessed the runoff contribution from different land use classes, and Verbeek [42] identified predictive variables of imperviousness to evaluate water retention services.

However, the validation of the urban water balance simulation based on a more detailed parameterization remains a challenging task. We believe that a single calibration/validation of the discharge is not enough to prove good model performance. To validate the different components of the water balance, intensive field work has to be fulfilled. Additional to the measurements described in [27], further experiments for the point validation of interception storage, evapotranspiration and infiltration are running. These experiments will help to validate the simulated water balance components for specific pixels within the catchment. However, this paper aims at showing the influence of including LAI maps in the WetSpa simulator and does not focus on validating the different water balance components. Our approach shows that using multi-resolution RS allows a location- and time-specific parameterization of a hydrological model. In a further step, this will allow quantifying the storage and retention capacity of a catchment more specifically and in a spatially-distributed way.

## 5. Conclusions

In this study, we monitor the urban vegetation in its heterogeneous and complex landscape to quantify its impact on hydrological processes and, more specifically, interception storage. We use a hyperspectral APEX image with a high resolution (2 m) in combination with frequent Proba-V satellite images at a lower spatial resolution (100 m) to characterize the seasonal variation of urban greenness. Based on our ground-truthing experiments, the use of remote sensing images for urban greenness characterization has been validated, and high resolution time series of LAI maps have been created. The LAI maps have an effect on the simulation of the interception storage capacity and the actual interception storage. They lead to an increase in simulated interception storage during winter months, but yield lower interception storage for summer events in the WMB catchment in 2015. The LAI maps enable a location- and time-specific parameterization of urban vegetation in the hydrological modeling framework. These remote sensing-based modeling tools provide quantitative information to assess the impact of policies and planning projects on the resilience of urban ecosystems.

**Supplementary Materials:** The following are available online at [www.mdpi.com/2072-4292/9/7/645/s1](http://www.mdpi.com/2072-4292/9/7/645/s1), Table S1: Calibrated WetSpa parameters; Table S2: User input file for WetSpa; Table S3: List of Proba-V images.

**Acknowledgments:** This research is co-funded within the framework of the UrbanEARS project SR/00/307 from the Belgian Federal Science Policy Office, Support to the Exploitation and Research in Earth Observation III (BELSPO STEREOIII), and the Belgian airborne calibration and validation sites for urban and forest (BELAIR-SONIA) project SR/03/333. The meteorological dataset is provided by the Royal Meteorological Institute (Uccle) and Flowbru (depot communal). We also want to thank Jeroen Degerickx for his contribution to the ground-truthing activities and Frederik Priem who provided the land cover map. English language editing was done by Steven Eisenreich. We further acknowledge the constructive feedback of the 3 reviewers and the efficient editing.

**Author Contributions:** C.W. and B.V. conceived and designed the ground-truthing experiments and the aggregation strategy. C.W. performed the ground-truthing and aggregation procedure. C.W. and B.V. analyzed the results, and prepared the structure of the manuscript. C.W. wrote the initial draft of the paper. B.V. and W.B. supervised the research and contributed to improving the manuscript prior to submission, W.B. was especially helpful with respect to the hydrological modeling. C.W., B.V. and W.B. prepared the final version of the manuscript taking into account the comments made by the reviewers.

**Conflicts of Interest:** The authors declare no conflict of interest.

## Abbreviations

APEX	Airborne Prism EXperiment
EnMAP	Environmental Mapping and Analysis Programme
LAI	Leaf area index
PAR	Photo-synthetically-active radiation
Proba-V	Project for OnBoard Autonomy-Vegetation
RMI	Royal Meteorological Institute
RS	Remote sensing
NDVI	Normalized difference vegetation index
NSE	Nash–Sutcliffe efficiency
WetSpa	Water and Energy Transfer between Soil Plants and Atmosphere
WMB	Watermaelbeek

## References

1. Konrad, C.P.; Booth, D.B. *Hydrologic Trends Associated with Urban Development for Selected Streams in the Puget Sound Basin, Western Washington USGS Water-Resources Investigations Report*; United States Geological Survey: Reston, VA, USA, 2002.
2. Pataki, D.E.; Boone, C.G.; Hogue, T.S.; Jenerette, G.D.; Fadden, J.P.M.; Pincetl, S. Ecohydrology Bearings-Invited Commentary Socio-ecohydrology and the urban water challenge. *Ecohydrology* **2011**, *4*, 341–347.

3. Carey, R.O.; Hochmuth, G.J.; Martinez, C.J.; Boyer, T.H.; Dukes, M.D.; Toor, G.S.; Cisar, J.L. Evaluating nutrient impacts in urban watersheds: Challenges and research opportunities. *Environ. Pollut.* **2013**, *173*, 138–149.
4. Braud, I.; Fletcher, T.D.; Andrieu, H. Hydrology of peri-urban catchments: Processes and modeling. *J. Hydrol.* **2013**, *485*, 1–4.
5. Salvatore, E.; Bronders, J.; Batelaan, O. Hydrological modeling of urbanized catchments: A review and future directions. *J. Hydrol.* **2015**, *529*, 62–81.
6. Im, S.; Kim, H.; Kim, C.; Jang, C. Assessing the impacts of land use changes on watershed hydrology using MIKE SHE. *Environ. Geol.* **2009**, *57*, 231–239.
7. Zhou, Y.; Wang, Y.; Gold, A.J.; August, P.V. Modeling watershed rainfall-runoff relations using impervious surface-area data with high spatial resolution. *Hydrogeol. J.* **2010**, *18*, 1413–1423.
8. Getachew, H.E.; Melesse, A.M. The Impact of Land Use Change on the Hydrology of the Angereb Watershed, Ethiopia. *Int. J. Water Sci.* **2012**, doi:10.5772/56266.
9. Carlson, T.N.; Arthur, S.T. The impact of land use—Land cover changes due to urbanization on surface microclimate and hydrology: A satellite perspective. *Glob. Planet. Chang.* **2000**, *25*, 49–65.
10. Andersen, J.; Dybkjaer, G.; Jensen, K.; Refsgaard, J.; Rasmussen, K. Use of remotely sensed precipitation and leaf area index in a distributed hydrological model. *J. Hydrol.* **2002**, *264*, 34–50.
11. Song, C. Optical remote sensing of forest leaf area index and biomass. *Prog. Phys. Geogr.* **2012**, *37*, 98–113.
12. Mass, C.F.; Ovens, D.; Westrick, K.; Colle, B.A. Does increasing horizontal resolution produce more skillful forecasts? The results of two years of real-time numerical weather prediction over the pacific northwest. *Am. Meteorol. Soc.* **2002**, *83*, 407–430.
13. De Paul, O.V. Remote sensing: New applications for urban areas. *Proc. IEEE* **2007**, *95*, 2267–2268.
14. Priem, F.; Canters, F.; Brussel, V.U. Synergistic use of LiDAR and APEX hyperspectral data for high-resolution urban land cover mapping. *Remote Sens.* **2016**, *8*, 787.
15. Parmehr, E.G.; Amati, M.; Taylor, E.J.; Livesley, S.J. Estimation of urban tree canopy cover using random point sampling and remote sensing methods. *Urban For. Urban Green.* **2016**, *20*, 160–171.
16. Launeau, P.; Kassouk, Z.; Debaine, F.; Roy, R.; Patrice, G.; Boulet, C.; Rouaud, J.M.; Giraud, M. Airborne hyperspectral mapping of trees in an urban area. *Int. J. Remote Sens.* **2017**, *38*, 1277–1311.
17. Hermans, C.; Smeyers, M.; Rodriguez, R.M.; Eyletters, M.; Strasser, R.J.; Delhay, J.P. Quality assessment of urban trees: A comparative study of physiological characterisation, airborne imaging and on site fluorescence monitoring by the OJIP-test. *J. Plant Physiol.* **2003**, *160*, 81–90.
18. Weng, Q.H.; Lu, D.S.; Liang, B.Q. Urban surface biophysical descriptors and land surface temperature variations. *Photogramm. Eng. Remote Sens.* **2006**, *72*, 1275–1286.
19. Heldens, W.; Heiden, U.; Esch, T.; Mueller, A.; Dech, S. Integration of remote sensing based surface information into a three-dimensional microclimate model. *ISPRS J. Photogramm. Remote Sens.* **2017**, *125*, 106–124.
20. Royal Meteorological Insititute (RMI). Available online: <https://www.meteo.be/meteo/view/nl/360955-Maandelijkse+normalen.html> (accessed on 31 March 2017).
21. Flowbru. Pluviometer Depot Communal. Available online: <http://flowbru.be/fr> (accessed on 5 November 2016).
22. Monteith, J.L. Evaporation and environment. Available online: <https://www.unc.edu/courses/2010spring/geog/595/001/www/Monteith65.pdf> (accessed on 20 June 2017).
23. Norman, J.M.; Jarvis, P.G. Photosynthesis in Sitca Spruce (*Picea sitchensis* (Bong) Carr.) V. Radiation penetration theory and a test case. *J. Appl. Ecol.* **1975**, *12*, 839–878.
24. Goudriaan, J. The bare bones of leaf-angle distribution in radiation models for canopy photosynthesis and energy exchange. *Agric. For. Meteorol.* **1988**, *43*, 155–169.
25. Norman, J.M. Modeling the complete crop canopy. In *Modification of the Aerial Environment of Plants*; American Society of Agricultural: St. Joseph, MI, USA, 1979; pp. 249–277.
26. Tucker, C.J. Red and photographic infrared linear combinations for monitoring vegetation. *Remote Sens. Environ.* **1979**, *8*, 127–150.
27. Verbeiren, B.; Khanh Nguyen, H.; Wirion, C.; Batelaan, O. An Earth observation based method to assess the influence of seasonal dynamics of canopy interception storage on the urban water balance. *Belgeo* **2016**, doi:10.4000/belgeo.17806.

28. Su, Z. Remote Sensing Applied to Hydrology: The Sauer River Basin Study. Ph.D. Thesis, Faculty of Civil Engineering, Ruhr University Bochum, Bochum, Germany, 1996.
29. Bindhu, V.; Narasimhan, B. Development of a spatio-temporal disaggregation method (DisNDVI) for generating a time series of fine resolution NDVI images. *ISPRS J. Photogramm. Remote Sens.* **2015**, *101*, 57–68.
30. Wang, Z.M.; Batelaan, O.; De Smedt, F. A distributed model for water and energy transfer between soil, plants and atmosphere (WetSpa). *Phys. Chem. Earth* **1997**, *21*, 189–193.
31. Liu, Y.B.; De Smedt, F. *WetSpa Extension, A GIS-Based Hydrologic Model for Flood Prediction and Watershed Management Documentation and User Manual*; Vrije Universiteit Brussel: Ixelles, Belgium, 2004; pp. 1–126.
32. Salvatore, E.; Bronders, J.; Batelaan, O. Enhanced model flexibility and coupling opportunities: The WetSpa model case. In Proceedings of the International Congress on Environmental Modelling and Software, Leipzig, Germany, 1–5 July 2012.
33. De Jong, S.M.; Jetten, V.G. Estimating spatial patterns of rainfall interception from remotely sensed vegetation indices and spectral mixture analysis. *Int. J. Geogr. Inf. Sci.* **2007**, *21*, 529–545.
34. Yuan, F.; Bauer, M.E. Comparison of impervious surface area and normalized difference vegetation index as indicators of surface urban heat island effects in Landsat imagery. *Remote Sens. Environ.* **2007**, *106*, 375–386.
35. Doherty, J.; Brebber, L.; Whyte, P. *PEST: A Unique Computer Program for Model-Independent Parameter Optimisation*; Institution of Engineers Australia: Canberra, Australia, 1994; p. 551.
36. Heiden, U.; Heldens, W.; Roessner, S.; Segl, K.; Esch, T.; Mueller, A. Urban structure type characterization using hyperspectral remote sensing and height information. *Landsc. Urban Plan.* **2012**, *105*, 361–375.
37. Van Stan, J.T.; Levia, D.F.; Jenkins, R.B. Forest canopy interception loss across temporal scales: Implications for urban greening initiatives. *Prof. Geogr.* **2014**, 41–51, doi:10.1080/00330124.2014.888628.
38. Holder, C.D.; Gibbes, C. Influence of leaf and canopy characteristics on rainfall interception and urban hydrology. *Hydrol. Sci. J.* **2017**, *62*, 182–190.
39. Sutanto, S.J.; Wenninger, J.; Coenders-Gerrits, A.M.J.; Uhlenbrook, S. Partitioning of evaporation into transpiration, soil evaporation and interception: A comparison between isotope measurements and a HYDRUS-1D model. *Hydrol. Earth Syst. Sci.* **2012**, *16*, 2605–2616.
40. Tang, S.; Luo, W.; Jia, Z.; Liu, W.; Li, S.; Wu, Y. Evaluating Retention Capacity of Infiltration Rain Gardens and Their Potential Effect on Urban Stormwater Management in the Sub-Humid Loess Region of China. *Water Resour. Manag.* **2016**, *30*, 983–1000.
41. Liu, Y.B.; Smedt, F.; Hoffmann, L.; Pfister, L. Assessing land use impacts on flood processes in complex terrain by using GIS and modeling approach. *Environ. Model. Assess.* **2004**, *9*, 227–235.
42. Verbeek, K. Imperviousness in Residential Neighborhoods: Assessing Spatio-Temporal Changes and Evaluating Water Retention Services. Ph.D. Thesis, Katholieke Universiteit Leuven, Leuven, Belgium, 2013.



© 2017 by the authors. Licensee MDPI, Basel, Switzerland. This article is an open access article distributed under the terms and conditions of the Creative Commons Attribution (CC BY) license (<http://creativecommons.org/licenses/by/4.0/>).